

Electronic structure of non-centrosymmetric superconductor LaPdSi₃ and its reference compound LaPdGe₃.

M. J. Winiarski, M. Samsel-Czekala

*Institute of Low Temperature and Structure Research, Polish Academy of Sciences,
Okólna 2, 50-422 Wrocław, Poland*

Abstract

Electronic structures of a superconductor without inversion symmetry, LaPdSi₃, and its non-superconducting counterpart, LaPdGe₃, have been calculated employing the full-potential local-orbital method within the density functional theory. The investigations were focused on analyses of densities of states at the Fermi level in comparison with previous experimental heat capacity data and an influence of the antisymmetric spin-orbit coupling on the band structures and Fermi surfaces (FSs) being very similar for both considered here compounds. Their FSs sheets originate from four bands and have a holelike character, but exhibiting pronounced nesting features only for superconducting LaPdSi₃. It may explain a relatively strong electron-phonon coupling in the latter system and its lack in non-superconducting LaPdGe₃.

Keywords: A. intermetallics, B. superconducting properties, E. electronic structure, calculation

1. Introduction

The investigations of specific conditions for superconductivity (SC) in non-centrosymmetric compounds were initiated in 2004 y. by the discovery of heavy-fermion SC in CePt₃Si with the superconducting critical temperature, $T_c = 0.75$ K [1]. The lack of inversion symmetry of a crystal introduces the so-called antisymmetric spin-orbit coupling (ASOC) that may lead to some unconventional character of SC, i.e., revealing a mixture of spin-singlet and spin-triplet pairings [2, 3].

Among compounds adopting the tetragonal BaNiSn_3 -type structure [4], the phenomenon of superconductivity has been reported for LaPdSi_3 ($T_c = 2.60\text{--}2.65$ K [5, 6]), LaPtSi_3 ($T_c = 1.52$ K [6]), LaIrSi_3 ($T_c = 0.77$ K [7]), LaRhSi_3 ($T_c = 2.16$ K [8]), BaPtSi_3 ($T_c = 2.25$ K [9]), CaPtSi_3 ($T_c = 2.3$ K [10]), CaIrSi_3 ($T_c = 3.3$ K [11]), SrPdGe_3 ($T_c = 1.49$ K [12]), and SrPtGe_3 ($T_c = 1.0$ K [12]). Despite the lack of centrosymmetry in the crystal structure, all these systems exhibit a typically BCS-like SC, except for CaIrSi_3 [11] having a weakly anisotropic superconducting gap. In turn, in this family, pressure-induced heavy-fermion SC has been detected in CeIrSi_3 ($T_c = 1.6$ K [7]), CeIrGe_3 ($T_c = 1.6$ K [13]), CeRhSi_3 ($T_c \approx 0.72$ [14]), and CeCoGe_3 ($T_c = 0.7$ [15]).

The LaPdGe_3 compound, recently reported by Troć et al. [16] as non-superconducting down to 0.3 K, can be considered as an isostructural reference system to the LaPdSi_3 superconductor. Interestingly, in the La-Pd-(Ge/Si) intermetallics, forming the layered $Immm$ -type structures, the substitution of Si with Ge atoms clearly improves the SC properties [17, 18, 19, 20, 21]. This effect may be connected with some modifications of specific Fermi surface (FS) features enhancing an electron-phonon coupling [22]. Therefore, in this paper, electronic structures of LaPdSi_3 and LaPdGe_3 are probed from first principles to find any differences that might explain an unexpected suppression of SC in LaPdSi_3 by the substitution of Ge into Si atomic positions. Analysed are the Sommerfeld coefficients, calculated from densities of states (DOSs) at the Fermi level (E_F), γ_e , and their experimental values of specific heat data, γ . This allows for an estimation of electron-phonon enhancement factors, λ_{ep} . Furthermore, the FSs topology of the $\text{LaPd}(\text{Si};\text{Ge})_3$ is compared to that of other compounds crystallising in the BaNiSn_3 -type structure as well as other non-centrosymmetric intermetallics, e.g. LaPtSi also exhibiting SC [23].

2. Computational details

Band structure calculations have been carried out with the full-potential local-orbital (FPLO-9) code [24]. The Perdew-Wang parametrisation (PW92 [25]) of the local density approximation (LDA) was applied in both scalar and fully relativistic modes. Experimental values of the lattice parameters of the BaNiSn_3 -type (space group $I4mm$) unit cell (u.c.), $a = 0.4352$ nm, $c = 0.9661$ nm for LaPdSi_3 [5] and $a = 0.45079$ nm, $c = 0.98478$ nm for LaPdGe_3 [16] were assumed. The atomic (Wyckoff) positions have been fully optimised.

Valence-basis sets were automatically selected by the internal procedure of FPLO-9. Total energy values of considered systems were converged with accuracy to 1 meV for the 16x16x16 \mathbf{k} -point mesh of the Brillouin zone (BZ), corresponding to 648 \mathbf{k} -points in the irreducible part of the BZ.

3. Results and discussion

The optimised (LDA) atomic positions of LaPdSi₃ and LaPdGe₃, collected in Table 1, only insignificantly differ from the available experimental data [16]. Interestingly, the accordance of the optimised Wyckoff positions for LaPdSi₃ with the experimental values for LaPdGe₃ is even better than of those for the Ge-based system itself. This effect is related to the fact that the LDA usually yields an underestimation of the u.c. volume. Therefore, the experimental lattice parameters of LaPdSi₃, used in our calculations, are more suitable for the experimental atomic positions of LaPdGe₃.

The calculated DOSs of considered here systems, presented in Fig. 1, exhibit a similar shape with narrow peaks of the La 4f states located well above the Fermi level. The contribution of the La 5d electrons is minor in the whole range of the valence bands below E_F . These bands down to -3 eV are dominated by the Si 3p electron orbitals. In turn, the contribution of the Pd 4d electrons forms wide peaks centred at around -4.5 eV and -4.0 eV for the Si- and Ge-based systems, respectively. In LaPdSi₃, deep valence bands of the Si 3s electron orbitals (not displayed) are separated by a pseudogap around -6 eV, whereas in LaPdGe₃ the Ge 4s electron contribution is located at slightly lower energies (below -7 eV), thus the band-energy gap between -6 eV and -7 eV is completely open. A similar total DOS dependence is also exhibited by other La-Pd-(Si/Ge) intermetallics (La₃Pd₄(Si;Ge)₄ [22]), but with a less dominant influence of the Si/Ge p states.

The DOS in the vicinity of E_F in both compounds is prevailed by p-electrons coming from Si/Ge atoms like in the case of CaPtSi₃ [26, 27]. The calculated DOS at E_F , $N(E_F)$ =1.42 states/eV/f.u., for LaPdSi₃ is only slightly higher than that obtained for LaPdGe₃ (=1.32 states/eV/f.u.), both suggesting a weakly metallic character, being common for intermetallic superconductors and for other members of the BaNiSn₃-type family of compounds.

The calculated, γ_e , and experimental, γ , values of the Sommerfeld coefficients and T_c , as well as electron-phonon enhancement factors, λ_{ep} , derived from the relation: $\gamma = \gamma_e(1 + \lambda_{ep})$, are gathered in Table 2. The $\lambda_{ep} = 0.09$ for LaPdGe₃ indicates a negligible electron-phonon coupling. Therefore, the

BCS-like SC in this compound is impossible. It is worth to note that for LaPdSi₃ the obtained λ_{ep} values (=0.40-0.59) are comparable to that of BaPtSi₃ (0.49) and, generally, adequate for weakly-coupled superconductors. However, despite the fact that for LaPdSi₃ both the T_c and γ_e are close to those of CaPtSi₃, λ_{ep} (=0.21) of the latter compound is significantly lower than that of LaPdSi₃ (=0.59). This effect is not observed for CaIrSi₃, where the relatively high T_c (=3.3 K) may better correspond to the high γ_e (= 4.6 mJ/mol/K²), but at the same time a reasonably moderate value of λ_{ep} (=0.43) is obtained. A similar value of λ_{ep} (=0.33) has been also reported for LaPtSi with $T_c = 3.35$ K [23]. The low λ_{ep} value for CaPtSi₃ can be partly explained by worse quality of the polycrystalline samples.

The influence of an antisymmetric spin-orbit coupling on band structure of LaPdSi₃ is presented in Fig. 2. Although the ASOC-driven splitting is distinct in some regions, e.g. for the conduction bands around the Γ point (band splitting is of about 0.2 eV), the overall impact of ASOC on the band structure at E_F and, hence, also the FS of LaPdSi₃ is almost negligible. The pronounced ASOC effects are exhibited mainly by valence bands originating from the Pd 4d electrons, yielding relatively large contributions below -3 eV. The fully relativistic calculations for BaPtSi₃ [9] and CaPtSi₃ [27] also revealed only slight changes of the scalar relativistic band structures around E_F . Oppositely, in LaPtSi, adopting a different non-centrosymmetric structure of the ThSi₂-type, the ASOC-driven FS modifications are significant [23].

The Fermi surfaces of LaPdSi₃ and LaPdGe₃, consisting of four holelike sheets, calculated in the fully relativistic approach, are depicted in Fig. 3. Since in both considered systems, the ASOC-driven band splitting is small at E_F , the lift of the Kramers degeneracy in pairs of I-II and III-IV FS sheets is also negligible and the sheets within each pair remain almost identical. Moreover, the differences between the overall shape of the FS sheets of the Si-based superconductor and its Ge-based reference compound seem to be irrelevant. Similarly complex FS sheets to III-IV sheets presented in Fig. 3 have been reported for BaPtSi₃ [9], CaPtSi₃ [26, 27], and LaIrSi₃ [7]. However, the cylindrical shape of III-IV sheets centered at the X points, is a unique feature of FS exhibited by LaPdSi₃ and LaPdGe₃. This FS topology is connected with a band gap region around E_F , clearly seen in Fig. 2, along the X - P - Γ_3 line.

The sections of III-IV FS sheets for studied here compounds, presented in Fig. 4, reveal an almost ideal FS nesting with a vector $\mathbf{q} = (0.5, 0.5) \times (2\pi/a)$,

spanning the cylindrical surfaces. It is worth to underline that for LaPdSi_3 this specific nesting vector spans a large area, since the cylinders are distinctly flatter than those of the other system. This feature remains the same for both scalar (not displayed) and fully relativistic FS results. One can suspect that the relatively strong electron-phonon coupling in the Si-based compound may be related to the additional nesting-driven anomaly in phonon dispersion curves. This issue requires a further experimental verification. The analogous idea has also been postulated for other Pd-based superconductor $\text{La}_3\text{Pd}_4\text{Ge}_4$ [22]. Furthermore, in the non-centrosymmetric LaPtSi the influence of a similar FS-nesting-driven anomaly on BCS-like SC has been confirmed by calculations of the phonon dispersion curves [23]. Meanwhile, such nested FS areas have not been reported for other BaNiSn_3 -type superconductors, thus this feature is generally not required for an occurrence of the SC in this family of compounds.

4. Conclusions

The electronic structures of superconducting LaPdSi_3 and its reference compound, LaPdGe_3 , have been studied from first principles. Although the calculated densities of states of both systems are very similar, the comparison of estimated here Sommerfeld coefficients with those determined from heat capacity data suggests negligible electron-phonon coupling in the non-superconducting LaPdGe_3 compound. Moreover, the strength of an anti-symmetric spin-orbit coupling in the both studied systems is comparable to that of other compounds crystallising in the BaNiSn_3 -type structure, but containing no heavy atoms. In turn, the spin-orbit splitting of their bands at the Fermi level is much weaker than that for LaPtSi (different non-centrosymmetric ThSi_2 -type structure). Finally, the Fermi surfaces of both investigated compounds exhibit four holelike sheets with unique nesting features, being more pronounced for the superconducting LaPdSi_3 than those for its reference Ge-based system. Since in this superconductor the nested area of the calculated FS is substantially larger and its estimated electron-phonon coupling is much stronger than those in the other compound, the latter effect can be caused by a nesting-driven electron-phonon anomaly that could be observed in the phonon dispersion curves. Hence, this issue requires further experimental investigations.

Acknowledgements

The authors acknowledge Prof. Ernst Bauer for valuable discussions. The calculations were performed in Wrocław Centre for Networking and Supercomputing (Project No. 158).

References

- [1] Bauer E, Hilscher G, Michor H, Paul Ch., Scheidt EW, Griбанov A et al. Phys Rev Lett 2004;92:027003.
- [2] Gor'kov LP, Rashba EI. Phys Rev Lett 2001;87:037004
- [3] Yuan HQ, Agterberg DF, Hayashi N, Badica P, Vandervelde D, Togano K, Sigrist M, Salamon MB. Phys Rev Lett 2006;97:017006.
- [4] Dorrscheidt W, Schafer H. J Less-Common Met 1978;58:209.
- [5] Kitagawa J, Muro Y, Takeda N, Ishikawa M. J Phys Soc Jpn 1997;66:2163.
- [6] Smidman M, Hillier AD, Adroja DT, Lees MR, Anand VK, Singh RP, Smith RI, Paul DM, Balakrishnan G. Phys Rev B 2014;89:094509.
- [7] Okuda Y, Miyauchi Y, Ida Y, Takeda Y, Tonohiro C, Oduchi Y et al. J Phys Soc Jpn 2007;76:044708.
- [8] Anand VK, Hillier AD, Adroja DT, Strydom AM, Michor H, McEwen KA, Rainford BD. Phys Rev B 2011;83:064522.
- [9] Bauer E, Khan RT, Michor H, Royanian E. Phys Rev B 2009;80:064504.
- [10] Eguchi G, Peets DC, Kriener M, Maeno Y, Nishibori E, Kumazawa Y, Banno K, Maki S, Sawa H. Phys Rev B 2011;83:024512.
- [11] Eguchi G, Wadati H, Sugiyama T, Ikenaga E, Yonezawa S, Maeno Y. Phys Rev B 2012;86:184510.
- [12] Miliyanchuk K, Kneidinger F, Blaas-Schenner C, Reith D, Podloucky R, Rogl P et al. J Phys Conf Ser 2011;273:012078.
- [13] Honda F, Bonalde I, Yoshiuchi S, Hirose Y, Nakamura T, Shimizu K, Settai R, Ōnuki Y. Phys C 2010;470:S543.

- [14] Kimura N, Ito K, Saitoh K, Umeda Y, Aoki H, Terashima T. Phys Rev Lett 2005;95:247004.
- [15] Settai R, Sugitani I, Okuda Y, Thamizhavel A, Nakashima M, Ōnuki Y, Harima H. J Magn Magn Mater 2007;310:844.
- [16] Troć R, Wawryk R, Griбанov AV. J Alloys Compd 2013;581:659.
- [17] Fujii H, Mochiku T, Takeya H, Sato A. Phys Rev B 2005;72:214520.
- [18] Fujii H. J Phys Condens Matter 2006;18:8037.
- [19] Mochiku T, Fujii H, Takeya H, Wuernisha T, Mori K, Ishigaki T, Kamiyama T, Hirata K. Phys C 2007;463-465:182.
- [20] Fujii H, Kasahara S. J Phys Condens Matter 2008;20:075202.
- [21] Kasahara S, Fujii H, Takeya H, Mochiku T, Thakur AD, Hirata K. J Phys Condens Matter 2008;20:385204.
- [22] Winiarski MJ, Samsel-Czekala M. J Alloys Compd 2013;546:124.
- [23] Kneidinger F, Michor H, Sidorenko A, Bauer E, Zeiringer I, Rogl P, Blaas-Schenner C, Reith D, Podloucky R. Phys Rev B 2013;88:104508.
- [24] FPLO9.00-34, improved version of the FPLO code by Koepernik K, Eschrig H. Phys Rev B 1999;59:1743.
- [25] Perdew JP, Wang Y. Phys Rev B 1992;45:13244.
- [26] Bannikov VV, Shein IR, Ivanovskii AL. JETP Lett. 2010;92:343.
- [27] Kaczkowski J, Jezierski A. J Alloys Compd 2011;509:6142.

Table 1: Calculated free atomic positions in unit cells of LaPdSi₃ and LaPdGe₃. Experimental values taken from reference [16] are given in parentheses.

atom		x/a	y/b	z/c
LaPdSi ₃ :				
La	2a	0	0	0.5978
Pd	2a	0	0	0.2505
Si	4b	0	1/2	0.3625
Si	2a	0	0	0.0000
LaPdGe ₃ :				
La	2a	0	0	0.5949 (0.5999)
Pd	2a	0	0	0.2480 (0.2496)
Ge	4b	0	1/2	0.3587 (0.3548)
Ge	2a	0	0	0.0000 (0.0000)

Table 2: Experimental, γ , and calculated, γ_e , values of the Sommerfeld coefficient, derived electron-phonon enhancement factors, λ_{ep} , and critical temperature values, T_c , for LaPdSi₃ and LaPdGe₃ as well as accessible data for other superconductors adopting the BaNiSn₃-type structure.

	γ_e ($\frac{mJ}{mol \cdot K^2}$)	γ ($\frac{mJ}{mol \cdot K^2}$)	λ_{ep}	T_c (K)
LaPdSi ₃	3.34	5.3 [5]	0.59	2.6 [5]
		4.67 [6]	0.40	2.65 [6]
LaPdGe ₃	3.11	3.4 [16]	0.09	-
BaPtSi ₃	3.9 [9]	5.8 [9]	0.49	2.25 [9]
CaPtSi ₃	3.3 [26, 27]	4.0 [10]	0.21	2.3 [10]
CaIrSi ₃	4.6 [26, 27]	6.6 [11]	0.43	3.3 [11]

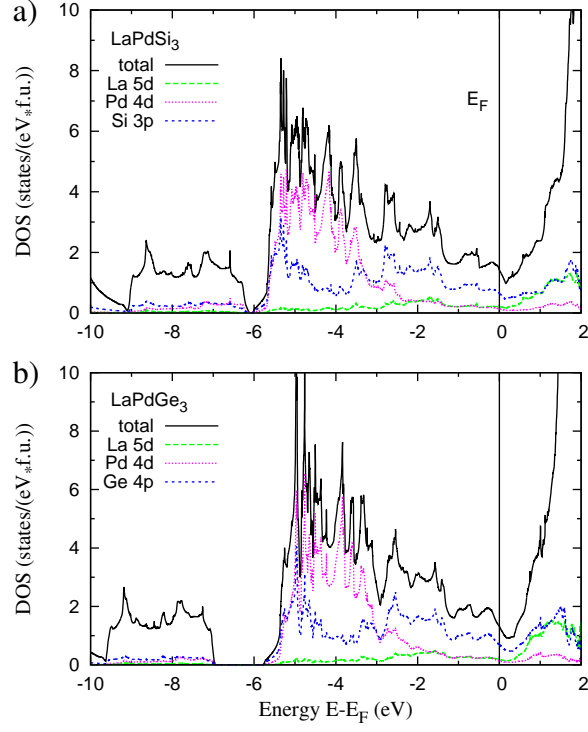


Figure 1: Total DOSs of LaPdSi₃ and LaPdGe₃ and their partial DOS contributions of La, Pd, and Si/Ge atoms, calculated in the fully relativistic approach.

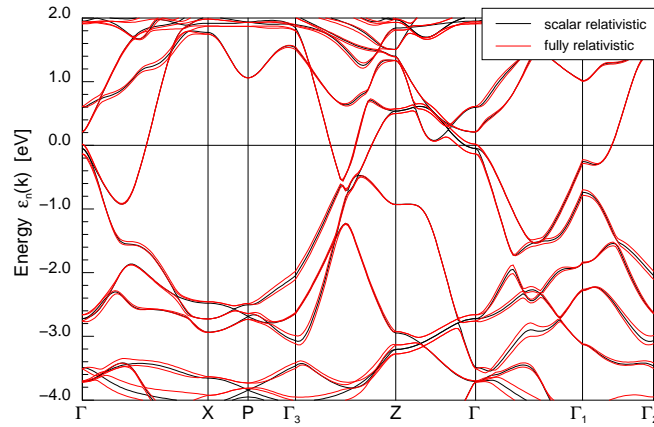


Figure 2: Calculated scalar and fully relativistic band structures of LaPdSi₃.

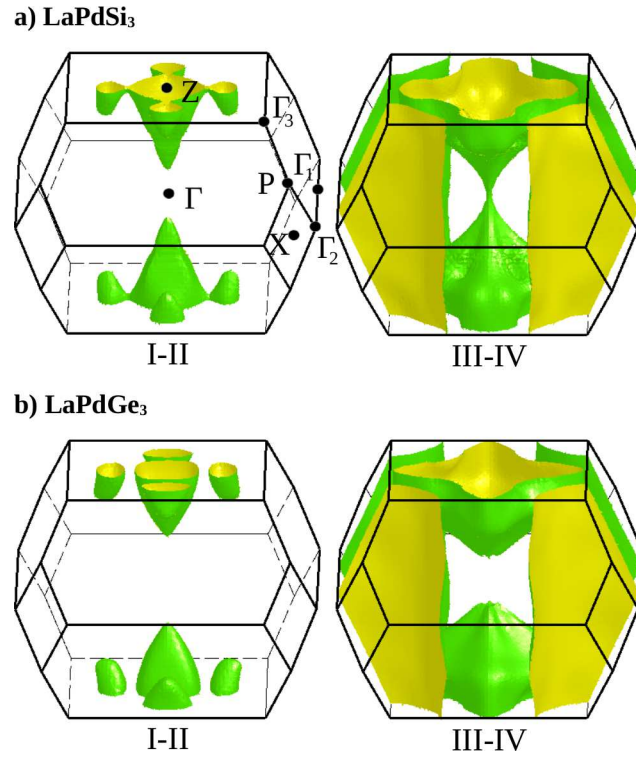


Figure 3: Calculated fully relativistic Fermi surfaces of LaPdSi₃ and LaPdGe₃, containing only holelike sheets. Note that the lift of the Kramers degeneracy of band pairs (I,II) and (III,IV) by the ASOC effects would be not visible in the scale of this figure, hence for each pair only single FS sheet is displayed.

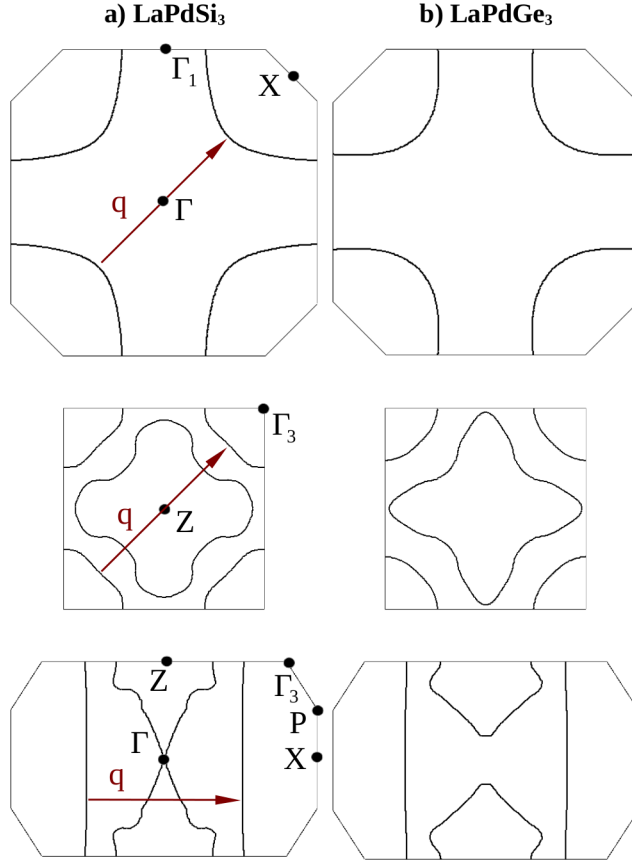


Figure 4: Fully relativistic sections of III-IV FS sheets (displayed in Fig. 3) in LaPdSi₃ and LaPdGe₃. Possible nesting vector $\mathbf{q} = (0.5, 0.5) \times (2\pi/a)$, spanning surfaces of the holelike cylinders, is marked by red arrows.